1. SCIENTIFIC RESEARCH

III. NEUTRON NUCLEAR PHYSICS

In 2016, in FLNP the scientific activity in the field of neutron nuclear physics was carried out in the following traditional directions: investigations of time and space parity violation processes in neutron-nuclear interactions; studies of the fission process; experimental and theoretical investigations of fundamental properties of the neutron; gamma-spectroscopy of neutron-nuclear interactions; atomic nuclear structure, obtaining of new data for reactor applications and nuclear astrophysics; experiments with ultracold neutrons, applied research using NAA. The scientific program to study the inelastic scattering of fast neutrons made into a separate project "TANGRA" was successfully implemented. A number of investigations in the field of fundamental physics and ultracold neutron physics were performed on the neutron beams of nuclear research centers in Germany, China, USA, France, Switzerland.

1. Experimental and methodological investigations

1.1. Investigation of the mechanism of fragment excitation and prompt neutron emission and gamma-ray cascades by simultaneous spectroscopy of fission fragments, neutrons and gamma-rays.

Spontaneous fission and fission induced by thermal and resonance neutrons are classical examples of low-energy fission, which occurs either at zero excitation energy of the fissioning nucleus or at excitation energies close to the fission barrier. Nuclear fission is a consequence of the collective motion of nucleons, which can be considered as a deformation of the surface of a nuclear liquid drop consisting of nucleons interacting via Coulomb and nuclear forces. The Strutinsky shell correction to the classical nuclear fission liquid-drop model has made it possible to create an effective calculation model of the multimodal (MM) fission. One of the most popular versions of these models parameterizes the changing (with increasing deformation) shape of a fissioning nucleus by quasi-spheroids connected by a rather thick neck at the prescission stage. The trajectories in the multidimensional deformation space are selected by minimizing the deformation energy of the fissioning system calculated by the specified method. Moreover, the shape symmetry of the fissioning system can change in the so-called trajectory bifurcation points. It should be noted that during the evolution, the fissioning nucleus overcomes the first barrier having a shape of a symmetrical "dumbbell", but to overcome the second barrier the configuration can be both symmetrical and asymmetrical. Along with it, energetically favorable configurations are those from a particular set of prescission shapes that determine the properties of fission modes (FM). A random neck rupture (RNR) leads to the separation of fission fragments because of the Coulomb repulsion. The primary fission fragments formed after the neck rupture are relatively "cold" and highly deformed. After the deformation energy is transformed to the core heating, prompt fission neutrons (PFN) are emitted.

The number of PFN, $\bar{\nu}(A,TKE)$, emitted by FF with the mass number A and the total kinetic energy TKE is directly related to the FF excitation spectrum. The measurement of the function $\bar{\nu}(A,TKE)$ allows one to obtain the characteristics of PFN averaged over A or TKE by integrating over the corresponding variable if the mass-energy distribution (MED) of FF – Y(A,TKE) is known. The examples of these averages together with the MED calibration are given below:

$$\bar{\nu}(A)=\frac{\int_0^\infty \bar{\nu}(A,TKE)Y(A,TKE)dTKE}{\int_0^\infty Y(A,TKE)dTKE}, \qquad \bar{\nu}=\int_0^\infty \bar{\nu}(A,TKE)Y(A,TKE)dTKE\,dA, \quad 200=\int_0^\infty Y(A,TKE)dTKE\,dA \qquad (1).$$

Thus, the experimentally measured multiplicity of PFN is a superposition of distributions $\bar{\nu}_i(A)$ of various FM with a realization probability p_i:

$$\bar{\nu}(A) = \frac{\sum_{i}^{N} p_i Y_i(A) \bar{\nu}_i(A)}{\sum_{A=0}^{A_{CN}} p_i Y_i(A)} \quad (2).$$

The experimental data analysis on the measurement of PFN allows one to obtain the following formula:

$$\bar{\nu}(A, TKE) = \left\{ \frac{\partial \bar{\nu}}{\partial TKE}(A)[TKE_{\max} - TKE(A)], \text{ if } TKE < TKE_{\max} \right\} \quad (3).$$

During 2013-2016 the data obtained in the experiments at the EC-JRC-IRMM Institute (Belgium) on the PNF emission in spontaneous fissions of ^{252}Cf were analyzed. As a result, the errors in the data analysis were identified and eliminated, which made it possible to explain the discrepancies in the results of the experiments with high and low neutron detection efficiency. In addition, a setup has been designed to study the prompt neutron emission and gamma-ray cascades for the fragments with defined masses in coincidence with PFN in the resonance neutron induced fission of ^{235}U. It consists of a double ionization chamber with Frisch grids, an NE-213-scintillator-based fast neutron detector, a pair of gamma-ray NaI-based scintillation detectors (**Fig. 1-III-1**).

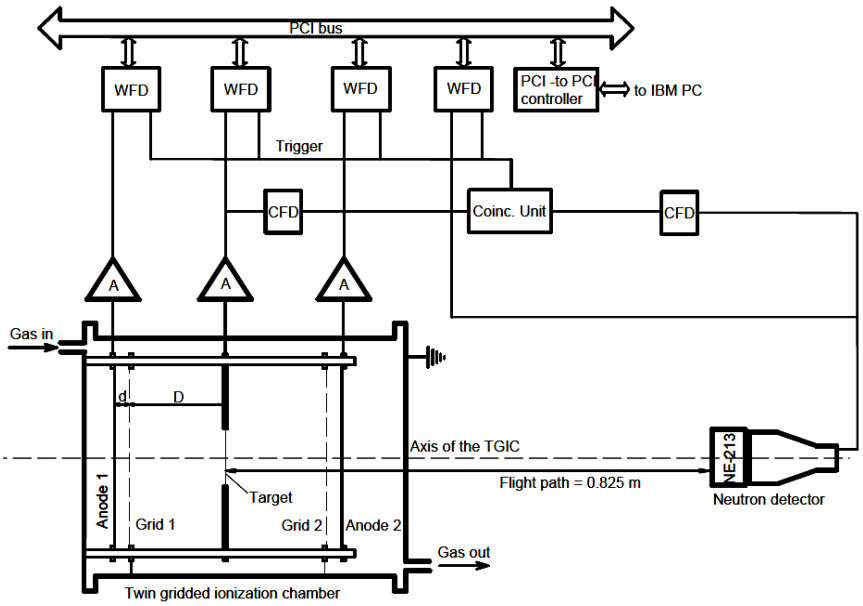

Fig. 1-III-1. *Schematic of the experimental setup. Gamma-detectors are not shown.*

The data acquisition system was implemented on the basis of an eight-channel system of synchronized pulse digitizers with a sampling rate of 250 MHz and amplitude resolution of 12 bits. The calibration experiments were carried out in the period from December 2015 to March 2016 on the IBR-2 thermal neutron beamline. At present, the data analysis and the setup upgrade involving the replacement of two NaI detectors with high-purity germanium detectors are in progress. Some results are presented in **Fig. 1-III-2, 1-III-3, 1-III-4**.

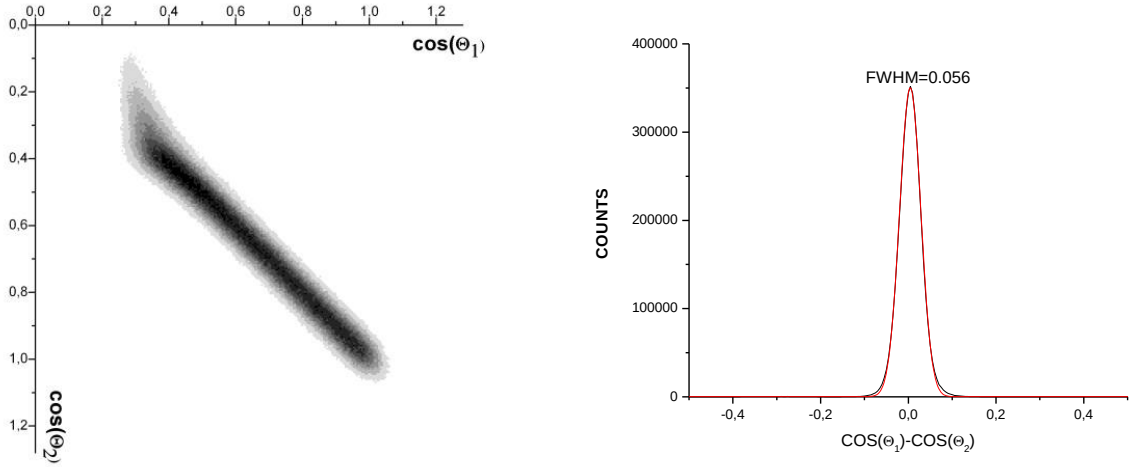

Fig. 1-III-2. *Demonstration of the measuring accuracy for FF angular distributions.*

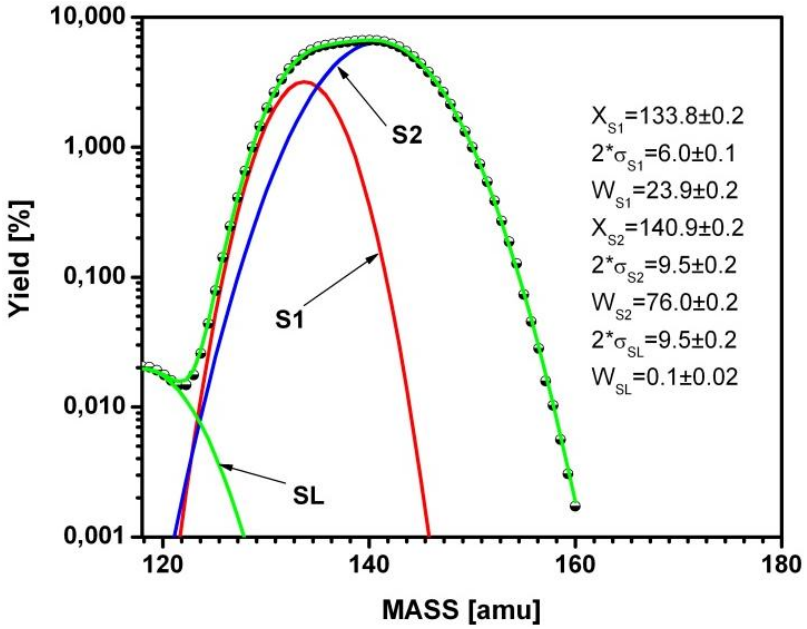

Fig. 1-III-3. *Fission modes for the mass distribution of thermal neutron-induced fission fragments of ^{235}U according to the calculations within the MM-RNR model.*

It also follows from the analysis of the experiment that for a fixed mass number A, $\bar{\nu}(A,TKE)$ becomes a linear function of TKE, so in practice it is sufficient to measure two functions $\bar{\nu}(A)$ and $TKE(A)$ to obtain $\bar{\nu}(A,TKE)$.

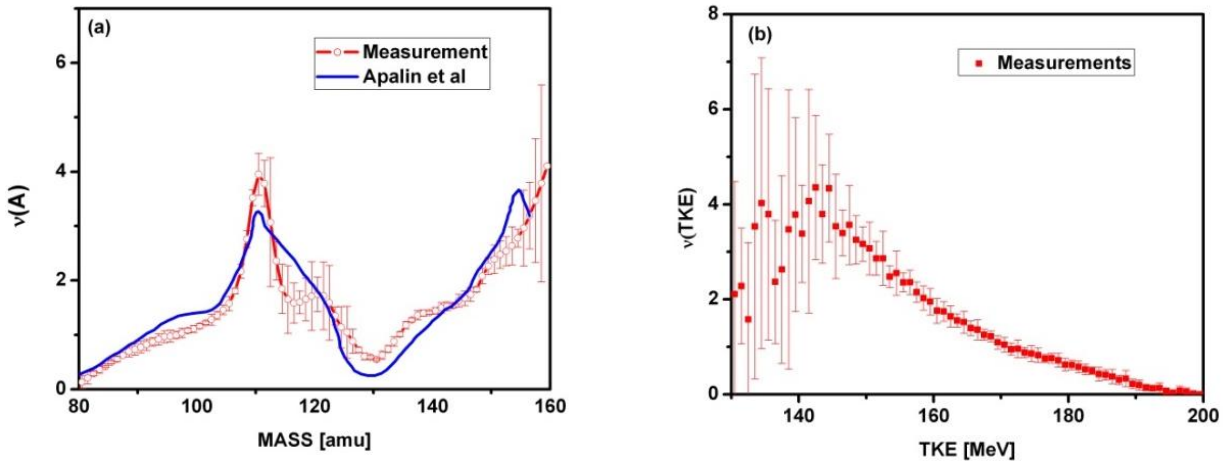

Fig. 1-III-4. *The average number of PFN as a function of mass (left) and TKE FF (right) measured in the experiment ^{235}U(n,f).*

The interest to the measurements of PFN multiplicity is primarily due to the fact that PFN carry information about the excitation energy of FF. In this regard, the information about the variations in the excitation energy depending on the FF mass is fundamental from the viewpoint of the fission process in the last stage of the evolution for the fissioning system from the saddle point on the potential energy surface to the point of rupture. In theoretical calculations of the fissioning nucleus excitation energy and its distribution between FF it is necessary to take account of a change in their excitation energy during the formation process. Recent experimental studies of the ^{237}Np(n,f) reaction in the range of incident neutron energy of 0.5 - 6.0 MeV have revealed that a growth of the incident neutron energy results in an increase in PFN emission mainly from a heavier fragment. This observation suggests that in the prescission configuration the excitation energy can be pumped from one forming FF to another through the neck. This process should have a strong impact on the PFN yield depending on the mass distribution between FF. The complete study of this effect requires more precise information about the level density in the forming FF, which for many years was calculated assuming that nucleons in the nucleus form a Fermi gas. This assumption, however, is not confirmed experimentally for the systems with low excitation energy. In this regard, it is necessary to conduct new experimental studies of the deexcitation process in FF by means of simultaneous measurements of PFN and prompt gamma-rays. For this purpose, a modern setup has been constructed, which provides simultaneous spectrometric measurements of FF masses, PFN and cascades of prompt gamma-rays. First experiments were carried out on the beam of thermal neutrons at IBR-2 at the end of 2015. At present, data processing and planning of new experiments at IREN are in progress.

1.2. Research of the dynamics of interaction between superfluid and normal phases of nuclear matter

The process of the phase transition of any nucleus under a change in its excitation energy can be theoretically studied in detail by analyzing the density of excited levels and partial widths of the nucleus transition between them. To obtain the reliable information, the accuracy in the determination of these functions at the level of no worse than a few tens of percent is required. Such an experimental level considering the possible existence of hidden (or undetermined so far) parameters of the process of the cascade gamma-decay of any compound state can only be achieved by using a modern mathematical model of the cascade decay of an arbitrary compound state.

The acquisition of coincidence statistics for the study of the process of cascade gamma-decay of the ^{172}Yb compound state at the DDR reactor in Dalat, Vietnam, has been completed. The accumulated gamma-gamma coincidences were processed in Dubna, FLNP JINR. The Cooper pair-breaking thresholds were determined up to the neutron binding energy. In **Fig. 1-III-5** the experimental intensity of the two-quantum cascades is compared with the results of the calculations in the framework of the existing representations of the nucleus as a statistical system of a Fermi gas and the Dubna model, which takes account of the interaction of the normal and superfluid phases of nuclear matter.

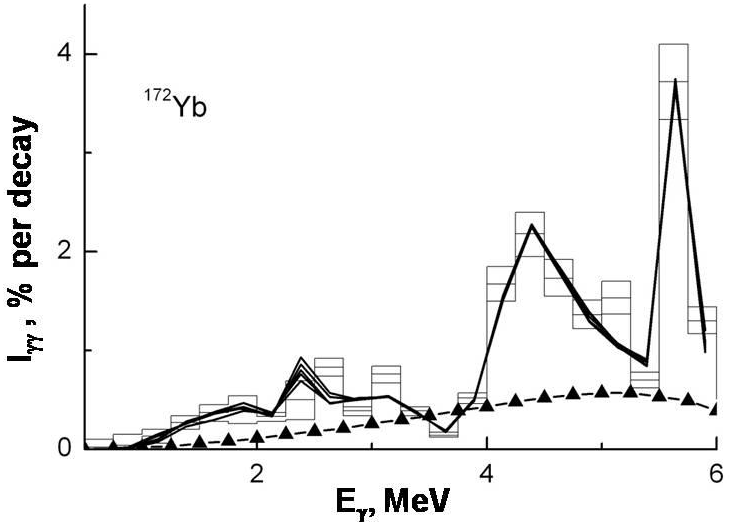

Fig. 1-III-5. *Dependence of the cascade intensity on the energy of primary transition. Histogram – experiment with its errors. Broken lines – results of the best fits for 5 options for the variable ratio of the capture cross-section in the resonances with spins J = 0 and J = 1. Triangles – cascade intensity calculated according to the conventional models of the level density and radiation strength functions of the statistical nucleus model.*

1.3. Investigations of (n,p), (n,α) reactions

On beamline №5 of EG-5, neutron-producing targets based on D(d,n)^{3}He (solid and gas targets) and ^{7}Li(p,n)^{7}Be reactions have been designed and tested during measurements. The development of a PIXIE-4 based electronic system for acquisition and storage of multidimensional data from an alpha-spectrometer at EG-5 has been completed and followed up by tests on a fast neutron beam.

The experimental and theoretical investigations of the (neutron, charged particle) reactions induced by fast neutrons have been conducted. The experiments were carried out at the Van de Graaf accelerators EG-5 in FLNP JINR and EG-4.5 of the Institute of Heavy Ion Physics of Peking University. Data on the reactions with the emission of charged particles induced by fast neutrons are of much interest for studying the mechanisms of nuclear reactions and atomic nuclear structure as well as in choosing engineering materials and in performing calculations in the development of new facilities for nuclear power engineering.

The analysis of the data from the measurements of the ^{144}Sm(n,α)^{141}Nd and ^{66}Zn(n,α)^{63}Ni reactions at E_n = 4.0, 5.0 and 6.0 MeV has been completed. The data have been obtained for the first time. For ^{66}Zn there have been no measurements in the neutron energy range of 0-20 MeV, for ^{144}Sm there have been only two measurements at around 14 MeV. The experimental cross-sections have been compared with the available libraries and calculations using the TALYS-1.6 code (**Figs. 1-III-6**).

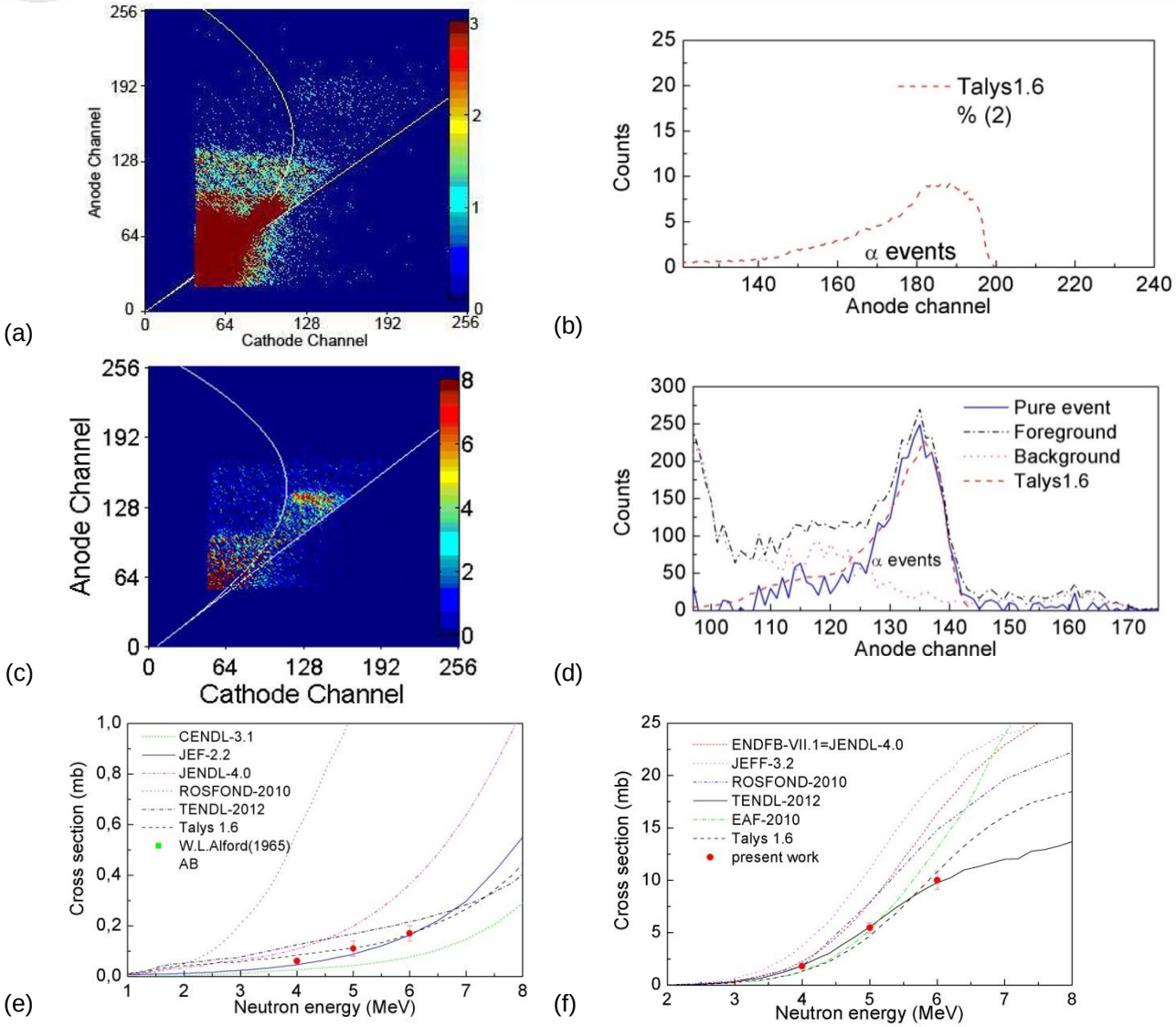

Fig. 1-III-6 (a) *2D spectrum of the $^{144}Sm(n,\alpha)^{141}Nd$ reaction at E_n = 4.0 MeV in the "forward" direction;* ***(b)*** *Spectrum from anode of the $^{144}Sm(n,\alpha)^{141}Nd$ reaction at E_n = 4.0 MeV in the "forward" direction;* ***(c)*** *2D spectrum of the $^{66}Zn(n,\alpha)^{63}Ni$ reaction at E_n = 5.0 MeV in the "forward" direction (with the background subtracted);* ***(d)*** *Spectrum from anode of the $^{66}Zn(n,\alpha)^{63}Ni$ reaction at E_n = 5.0 MeV in the "forward" direction;* ***(e)*** *Cross-section of the $^{144}Sm(n,\alpha)^{141}Nd$ reaction in comparison with the existing measurements and estimates for the neutron energy range from 1.0 to 8.0 MeV;* ***(f)*** *Cross-section of the $^{66}Zn(n,\alpha)^{63}Ni$ reaction in comparison with the existing measurements and estimates for the neutron energy range from 2.0 to 8.0 MeV.*

A systematic analysis of our experimental cross-sections of the (n,α) reaction in the energy range from 4 to 6.5 MeV has been performed. The dependence of the cross-sections on the parameter (N–Z+0.5)/A in this energy range has been observed and explained in the framework of the statistical model. At the same time, formulas of the statistical model give overestimated values for the absolute cross-sections of the (n,α) reaction. This difference between the theoretical calculations and experiment can be eliminated by introducing a clustering factor for alpha particles in the nucleus, Wp/α = 4.5. The results of the analysis can be used in astrophysical calculations, e.g. for the s-process, helium burning, and also allow one to estimate the cross-sections of unstable isotopes for which the measurements are difficult or impossible.

1.4. Measurements of gamma-spectra and angular distributions of gamma-rays for various nuclei using the tagged neutron method

In the framework of the "TANGRA" project, the angular correlations of γ-rays and neutrons, as well as gamma-spectra produced in the inelastic scattering of 14.1 MeV neutrons by various nuclei have been measured. These measurements are aimed at determining the partial cross-sections of the formation of nucleus excitation levels with the corresponding gamma-lines in inelastic neutron scattering reactions, as well as spin characteristics of these levels in the given reaction. This information is important for further development of the method of elemental analysis using tagged neutrons, in particular, to create a local database of characteristic gamma-rays for a broad set of elements, and for a detailed study of inelastic scattering reactions of fast neutrons by these nuclei. **Figure 1-III-7** shows samples for measuring gamma-spectra at the TANGRA facility.

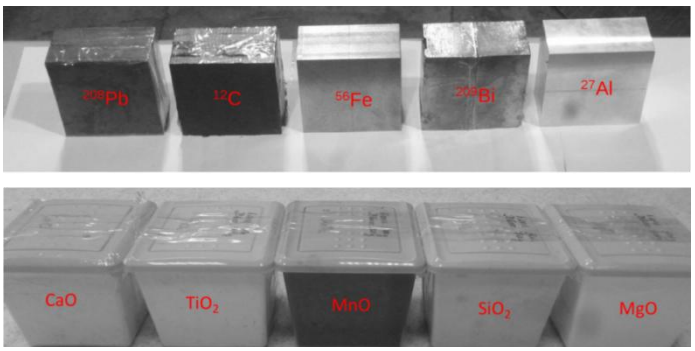

Fig.1-III-7. *Samples for measuring gamma-spectra at the Tangra facility.*

A scheme of the experiment is presented in **Fig. 1-III-8**. As a source of 14.1-MeV neutrons we used a portable neutron generator ING-27 developed and manufactured at the N.L.Dukhov Russian Institute of Automatics (VNIIA). To form a flux of tagged neutrons, the generator comprises a built-in double-sided silicon strip detector with eight mutually perpendicular strips on each side, which form an 8x8 matrix of 6x6 mm^2 pixels. The alpha-detector is located at a distance of 100 mm from the tritium target of the neutron generator (NG) and intended to detect 3.5-MeV alpha-particles produced in the reaction $(d+t \rightarrow \alpha(3{,}5\ \mathrm{MeV}) + n(14{,}1\ \mathrm{MeV})$ .Characteristic gamma-rays from the irradiated targets were detected by 22 detectors on NaI(Tl) crystals shaped as hexagons (distance between crystal faces – 85 mm, crystal height – 200 mm). The γ-ray detectors were arranged perpendicularly to the horizontal plane in a circle of radius of 370 mm with a target under study placed in its center. The angle between the axes of two adjacent NaI(Tl) crystals in the horizontal plane was 15°.

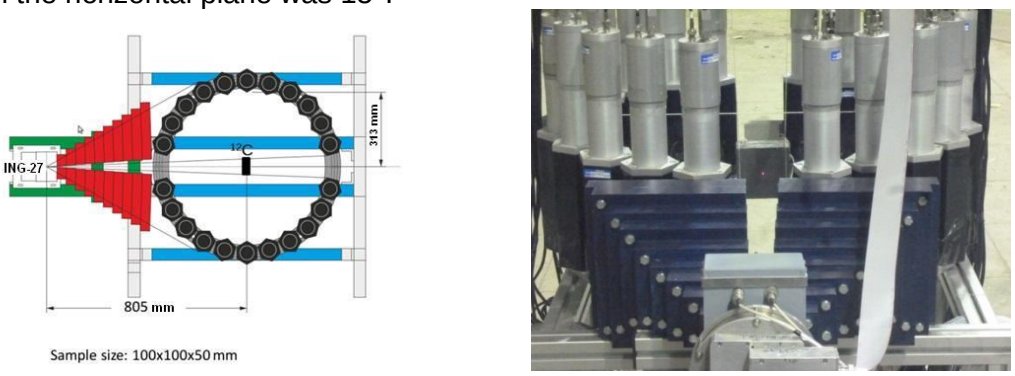

(a) (b)

Fig. 1-III-8. *A general view of the experiment* ***(a)*** *and the setup* ***(b)***

As an example, **Figure 1-III-9** shows spectra of gamma-rays measured by the detector positioned at an angle of 30° for different samples. A detailed analysis of the obtained experimental data is scheduled for 2017.

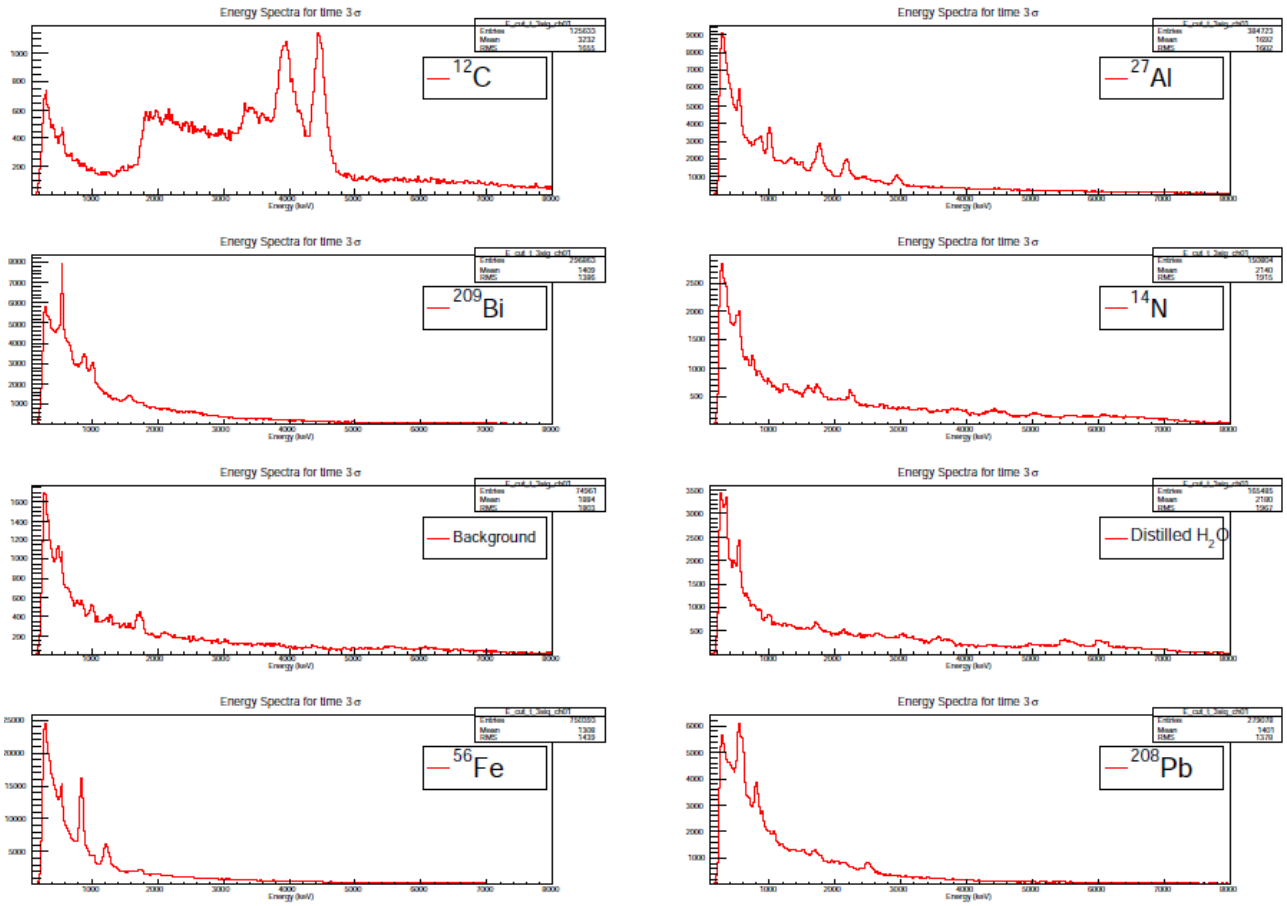

Fig. 1-III-9. *Energy distribution of the events detected by the γ-detector positioned at an angle of 30°.*

1.5. Measurement of T-odd effects in ^{235}U fission on a hot source of polarized neutrons

In the framework of the FLNP-ITEP-FRM2 collaboration a series of experiments have been continued to measure the ROT-effect in the emission of prompt γ-rays and neutrons in the binary fission of ^{235}U and ^{233}U induced by polarized cold neutrons. The experiments were carried out on the POLI instrument at the FRM-2 reactor (Garching, Germany).

For these experiments a neutron spin control system based on rectangular coils in magnetic screens was developed. The system to control the polarization vector of the neutron beam with a high accuracy (10^{-4}) was developed among other methods in Dubna in 1997-1999. This method uses the neutron spin precession in a magnetic field. The developers of the method had positive experience in using such systems (coils) to control the direction of neutron polarization. In the early eighties, they used the coils in magnetic screens for epithermal and resonance neutrons.

The main advantage of such coils is high magnetic field homogeneity in combination with small dimensions. Soft magnetic screens of the coils made of an alloy with high permeability allow one to use these devices as portable boxes with homogeneous magnetic fields (BHF). A simple

construction of the coil is shown in **Fig. 1-III-10** it consists of a rectangular coil frame with grooves to ensure high precision in winding aluminum wires.

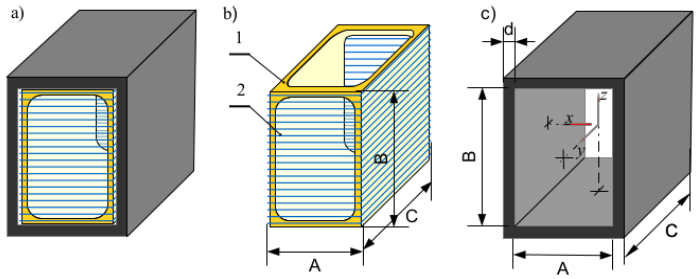

Fig. 1-III-10. *Box with homogeneous magnetic field: a) box (BHF); b) rectangular coil frame (1) aluminum coils (2), and c) external magnetic screen. A, B, C – coil dimensions. D – yoke thickness.*

When a neutron enters the coil with a homogeneous magnetic field *B*, it starts to precess around the direction of the field with a frequency *f* proportional to the external field. In particular, for a neutron with energy E = 0.3 eV the spin rotates by 90° at *l* = 52 *mm*, *B* = 4π *G* and *I* = 0.5 *A*.

The schematic of the experiment with the location of all coils to control polarization is presented in **Fig. 1-III-11**.

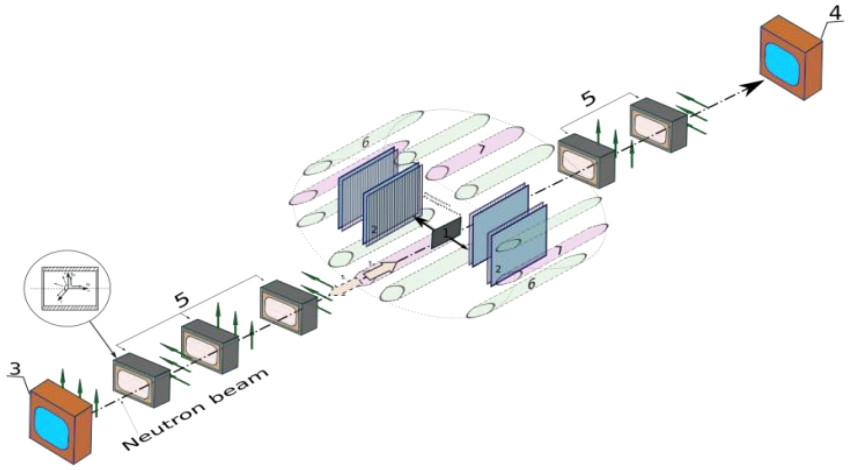

Fig. 1-III-11. *Schematic of the experiment. 1) target; 2) multi-wire proportional chamber for the detection of fission fragments; 3) polarizer; 4) analyzer; 5) rectangular coils in magnetic screens (arrows show the magnetic field direction); 6) plastic scintillation detectors; 7) scintillation detectors of gamma-rays and neutrons.*

Cells with polarized ^{3}He (length of approximately 13 cm and pressure of about 2.5 atm) were used as a polarizer and analyzer. The cells were placed in rectangular coils with a magnetic screen and homogeneous magnetic field providing ^{3}He relaxation time in the cells of about 40 hours. To control polarization, five similar coils of smaller dimensions allowing one to vary the current magnitude and direction in each of them were used, which made it possible to provide any neutron polarization direction in a given point along the neutron beam. One of the coils was used as a spin-flipper with a spin-flip frequency of the order of 1.3 s.

The experimental setup at the POLI instrument of the FRM2 reactor is shown in **Fig. 1-III-12**.

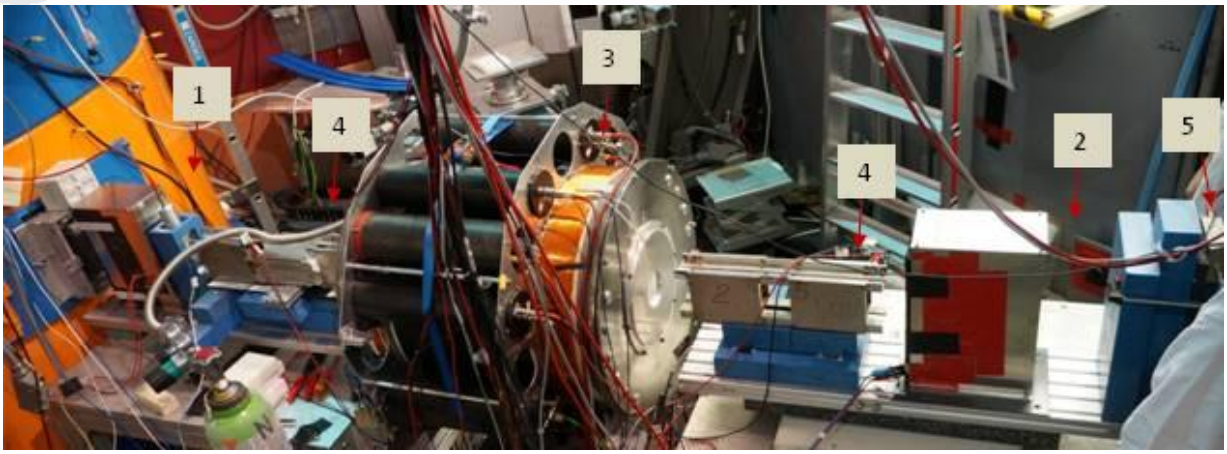

***Fig. 1-III-12**.Setup for measuring the ROT-effect at the POLI instrument (FRM2, Garching). 1 – neutron polarizer, 2 – analyzer, 3 – fission chamber surrounded by gamma-ray and neutron detectors, 4 – polarization control coils, 5 – neutron counter for measuring polarization*

A beam of 0.3-eV neutrons was monochromatized by a mosaic single crystal diffractometer and focused on the target. A neutron polarizer on the basis of a polarized ^{3}He cell with an average polarization of ~70% was placed between the diffractometer and the target. The polarized neutron flux density at the target was ~ 5 x 10^6 n $cm^{-2}s^{-1}$. The polarization was controlled by a similar analyzer and measured by a neutron counter. Since the neutron beam should be horizontally polarized at the target and the polarization of neutrons after ^{3}He cells was vertical, rectangular coils in magnetic screens providing polarization control were installed on both sides of the chamber. The direction of the magnetic field in the first coil changed every 1.3 s, which created an analogue of a spin-flip and allowed us to measure the difference effect.

Fragments were detected by fast multi-wire detectors and could be separated into light and heavy ones by the time of flight. Gamma-rays and neutrons were detected by scintillation counters (plastic, NaI(Tl)) placed at specific angles to the direction of emission of the fragments. The so-called ROT-effect (effect of rotation of the fissioning system in or against the direction of the angular momentum transferred by a polarized neutron) for gamma-rays and neutrons was measured. Neutrons were separated from gamma-rays by the time-of-flight method.

The effect was measured for 9 days. As a result, the effect values (averaged over all detector position angles) were obtained:

- for gamma-rays: $(-4.6 \pm 2.7) \times 10^{-5}$;
- for neutrons: $(2.7 \pm 2.9) \times 10^{-5}$.

For gamma-rays, the value of the ROT effect differs from zero at the level of 2σ, for neutrons no statistically significant effect in the limits of errors was observed.

In 2017, a new experiment is planned, in which we expect to observe the effect or determine its upper limit with the accuracy comparable to that obtained on the cold neutron beam.

1.6. Measurement of the coefficients of P-odd angular correlations in the reactions of cold polarized neutrons with light nuclei.

The measurement of P-odd asymmetry in the emission of α-particles in the ^{10}B(n,α)^{7}Li reaction was carried out on the cold polarized neutron beam of the PF1B instrument at the ILL reactor (Grenoble, France). A 24-section ionization chamber with insensitive gas gaps was used as a detector of α-particles. The P-odd asymmetry value was found to be $\alpha_{P-odd}^{^{10}B,\alpha} = -(11.2 \pm 3.4) \cdot 10^{-8}$.

The result has been obtained for the first time in the world. This is only the second nucleus after ^{6}Li for which the P-odd effect was discovered.

1.7. Experiment to obtain a focused beam of very cold neutrons using a reflector of diamond nanoparticles

Ultracold neutrons (UCN) and very cold neutrons (VCN) intensively interact with nanoparticles due to the fact that the neutron wavelength and the particle size are of the same order of magnitude – a few nanometers, therefore, the cross-section of elastic coherent neutron scattering by particles is high. In [1] for the first time VCN with velocities of 40-160 m/s were reported to be stored in a trap with walls composed of diamond nanoparticles and effectively reflecting such neutrons.

One of the practical applications of nanoparticle reflectors can be a sharp increase in the VCN yield from the source, if we manage to form a narrow beam from the isotropic distribution and direct it to a neutron guide. In order to determine the possibility of the formation of such beams, a specialized experiment (scheme is shown in **Fig. 1-III-13**) was carried out.

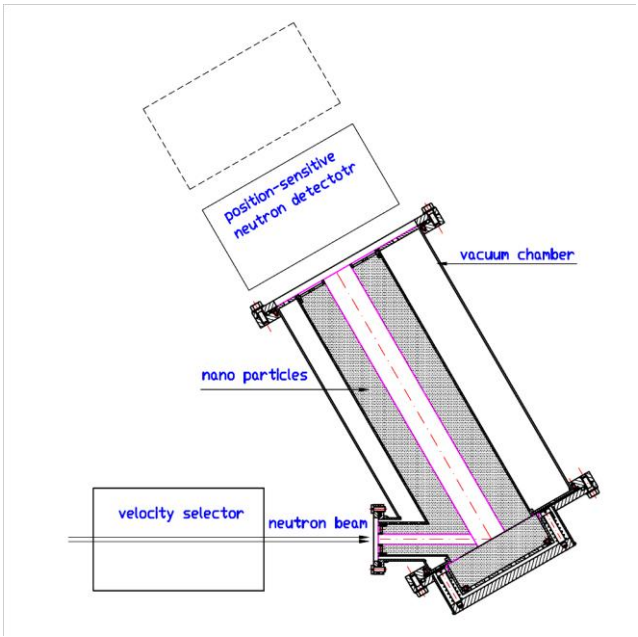

Fig. 1-III-13. *Scheme of the experiment.*

A beam of very cold neutrons (velocities 40-90 m/s) with a diameter of 8 mm passes through a velocity selector (with a resolution from 5% to 20%) and comes to the bottom of the trap through the inlet opening (∅ 10 mm). The trap is a thick-walled tube with an inner diameter of 30 mm and length of 30 cm. The walls of the tube consist of nanodiamond powder. Neutrons confined in a trap can be detected by a position-sensitive detector mounted on its exit end. By changing the distance from the trap exit to the detector, it is possible to measure the number of emitted neutrons and their angular distribution.

The preliminary results have shown that the number of escaping neutrons is ~1-2% of the number of neutrons entering the trap, with the yield increasing as the neutron energy decreases. The beam formed has an angular divergence of 10^{-2}-10^{-3} rad. These results indicate that the

covering of a VCN source with a nanoparticle reflector can result in a tenfold increase in the number of VCN in the neutron guide.

1.8. Experiment to study quasi-specular reflection of cold neutrons from the surface of nanopowder

The scattering of particles/rays at small angles in a medium (small-angle scattering) leads to the fact that for a beam of particles/rays falling on the medium at a glancing angle the angular distribution of reflected particles/rays has a pronounced maximum at an angle close to the angle of incidence, i.e. the so-called quasi-specular reflection is observed. A similar situation exists for neutrons when falling at a small angle on a medium with the effective small-angle scattering. Nanoparticles with a size of a few nanometers can effectively scatter cold neutrons at small angles. Therefore, for cold neutrons falling on the surface of a nanopowder a quasi-specular reflection (first described in [2]) can also be observed.

We experimentally measured the parameters of this phenomenon using the reflection of neutrons from a nanodiamond powder. For this purpose, we measured the dependence of the angular distribution of reflected neutrons for different wavelengths of incident neutrons and different angles of incidence (1°, 2°, 3° and 4°) of the neutron beam on the surface. The measurements were performed for a powder of nanoparticles of different sizes. The preliminary results of the measurements are presented in **Figs. 1-III-14 (a) and (b).**

(a)

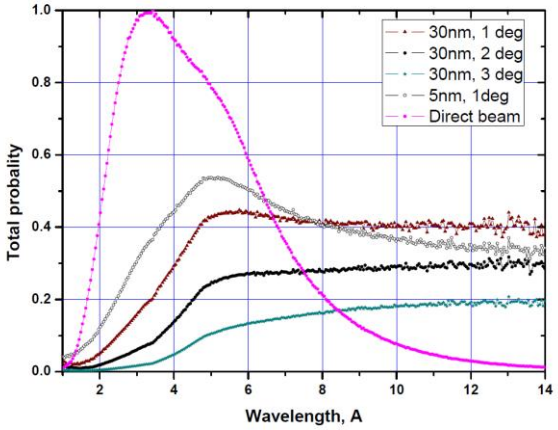

(b)

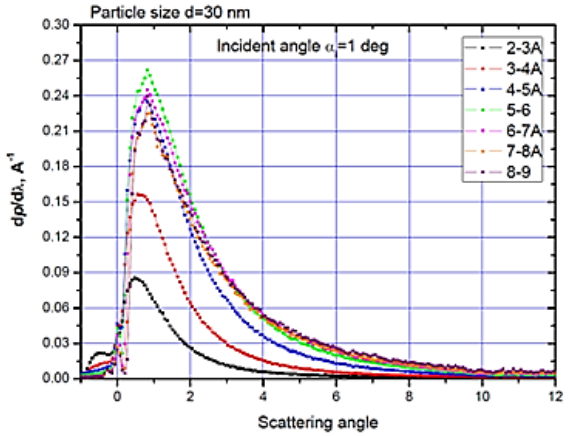

Fig. 1-III-14. (a)*Total probability of reflection from the surface of nanopowders as a function of neutron wavelength for angles of incidence of 1°, 2° and 3°. The data for powders of two kinds of nanoparticles with an average size of 30 nm and 5 nm are presented.****(b)*** *Angular distribution of neutrons reflected from the surface of a powder of nanoparticles with an average size of 30 nm for different neutron wavelengths.*

From the data presented in **Fig. 1-III-14** it can be clearly seen that for neutrons with longer wavelengths a more efficient reflector is that with large nanoparticles, for neutrons with shorter wavelengths – with small nanoparticles.

The findings can help in the construction of primary sections of mirror neutron guides for VCN and CN placed near a reactor core, which can significantly increase the neutron emission of the sources into the neutron guides.

1.9. Neutron diffraction by a moving grating

In the Institute of Laue-Langevin a new experiment to obtain UCN spectra for the diffraction by a moving grating (DMG) was performed. Its main purpose was to verify a theoretical prediction that at a certain height of the grating profile a significant suppression of the zero-order diffraction

may occur with a corresponding increase in the intensity of the lines of other orders. If this prediction is true, then by choosing a proper grating profile one can enhance the efficiency of the neutron energy transfer during DMG. The measurements of the spectra were carried out using the previously designed time-of-flight Fourier diffractometer of UCN (**Fig. 1-III-15**).

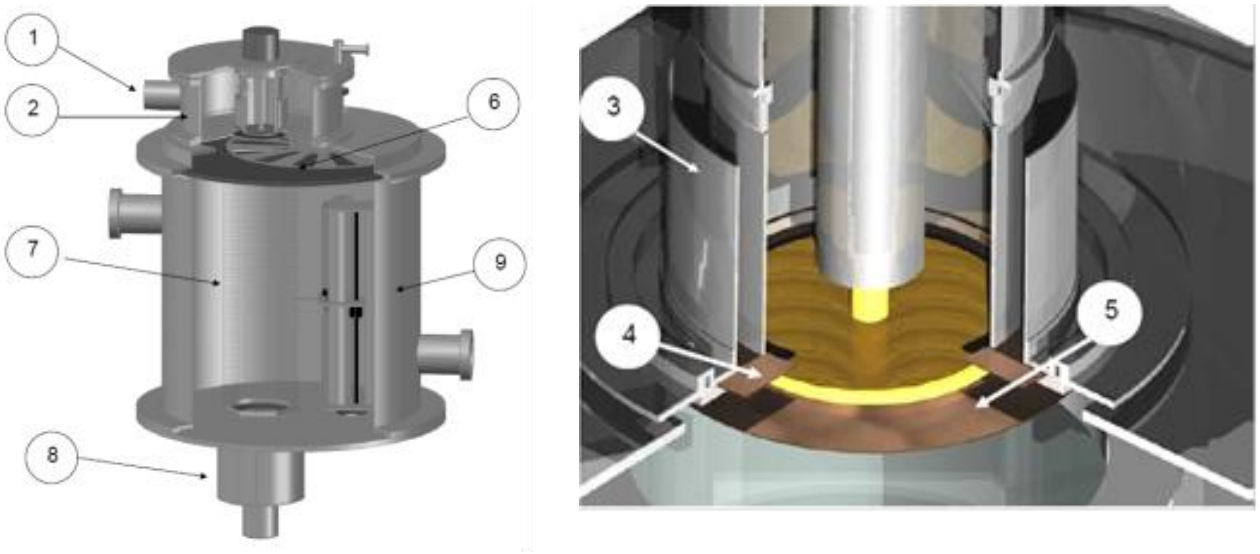

Fig. 1-III-15*. Time-of-flight Fourier spectrometer: general view (left) and its upper part (right): 1 – leading neutron guide, 2 - inlet chamber, 3 - circular hall, 4 - filter-monochromator, 5 - grating 6 - rotor of Fourier chopper, 7 - vertical glass neutron guide, 8 - detector, 9 - vacuum chamber.*

A new grating prepared as previously on the periphery of a silicon disc had 84000 radial grooves with a profile depth of 0.22 μm. The grating profile was analyzed using atomic force microscopy (**Fig. 1-III-16**). The spectra were obtained for four rotational speeds of the grating. It was found that the teeth and grooves of the grating follow rather a trapezoidal profile than a rectangular one.

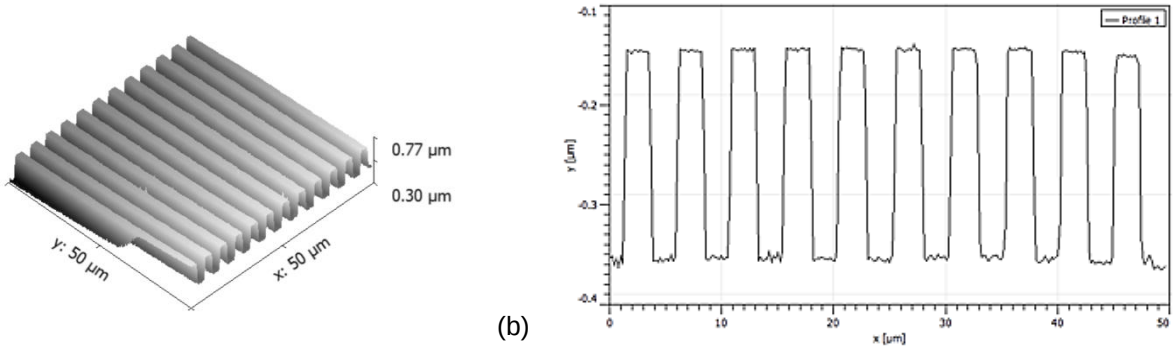

(a) (b)

Fig.1-III-16. *3D image of a grating fragment obtained by atomic force microscopy (left) and its profile (right). The scales on the two axes are substantially different.*

The comparison with the spectrum obtained for the grating with a less deep profile (**Fig. 1-III-17**, two bottom graphs) demonstrates the validity of the prediction about the possibility of a significant suppression of zero-order intensities. This is the main result of this experiment.

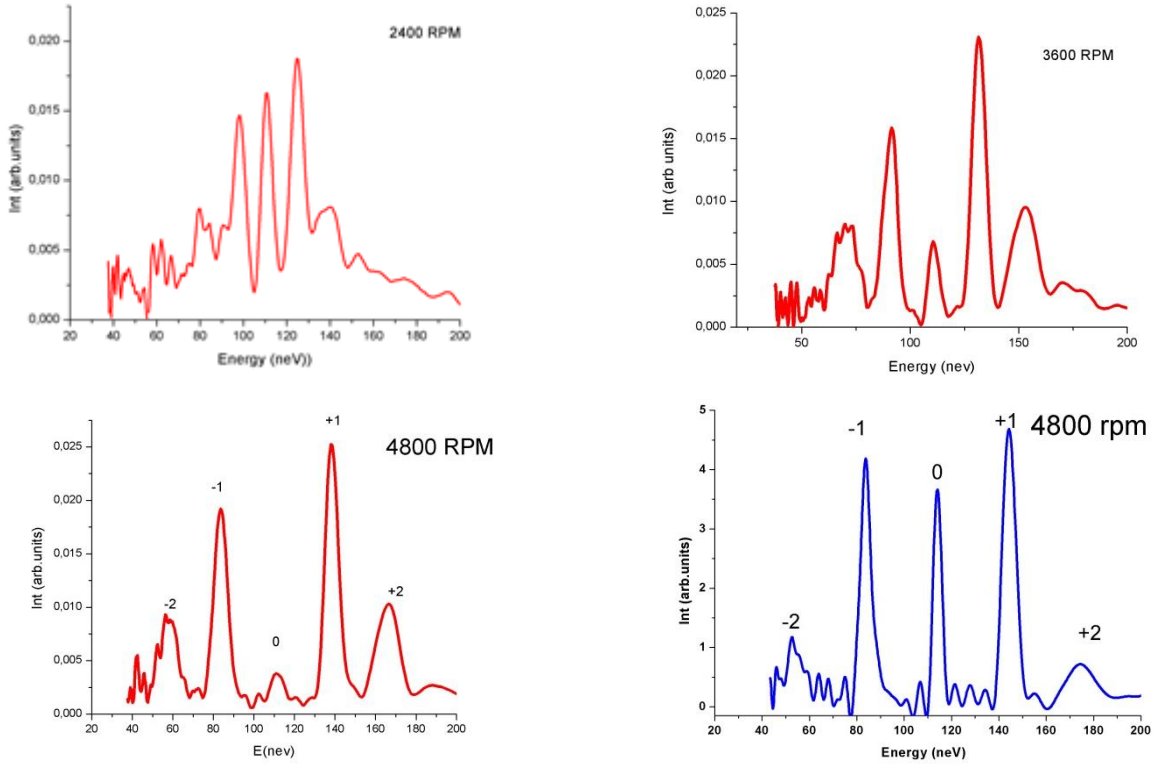

Fig. 1-III-17. *Neutron spectra of diffraction by a moving grating with deep profile for three rotational speeds of the grating (2016). The bottom right figure shows the spectrum obtained in 2014 for the grating with a smaller profile depth. It can be seen that zero-order intensities are significantly different.*

At the same time, the experimental spectra are not in full agreement with the results of the calculations. A reason for this discrepancy is not well understood for the moment, and its clarification requires a more thorough theoretical analysis of the DMG phenomenon together with the search for possible systematic effects inherent in the time-of-flight Fourier diffractometer of UCN.

1.10. Analysis of the accuracy of UCN time-of-flight measurement by Fourier spectroscopy

We are currently considering the possibility of a new experiment to test the weak equivalence principle. The experiment is based on the measurement of the time of flight of neutrons belonging to several diffraction orders in DMG. In this experiment, it will be necessary to ensure the accuracy of the time measurement at the level of 10 μs. A test experiment was carried out to determine the possibility of using for this purpose a Fourier-diffractometer of UCN. The analysis showed that in the existing diffractometer presented above in **Fig. 1-III-15** there are sources of systematic effects leading to an absolute error in the measurement of time of flight, which reaches in some cases several hundred microseconds. Along with it, when measuring the time-of-flight difference there were no such problems.

In the considered experiment, the energy spectrum of UCN was formed by a five-layer planar nanostructure — neutron Fabry-Perot interferometer — placed in a vertical neutron guide. The interferometer transmitted UCN with a narrow energy spectrum with an average energy of about 114 neV. The time of flight of neutrons when falling down was 114 ms. It was measured for two positions of the interferometer differing in height by 5 mm. At the same time the neutron energy

changed by about 5 neV due to the Earth's gravity and the change in the time of flight was about 280 μs. The aim of the experiment was to measure the difference in the time of flight at two positions of the interferometer.

The procedure of accuracy evaluation was as follows. Two time-of-flight spectra were obtained for two positions of the monochromator. By fitting single peaks in each of the two spectra after the Fourier synthesis, a value of 290 μs was found for the difference in the time-of-flight values with uncertain accuracy at this step. Then, each of the raw data sets was divided into 30 groups and each group of data was considered as a result of an independent measurement. For each group its own spectrum with a single line was built using the Fourier synthesis and the line positions on the time scale were determined. The difference between the two averaged time-of-flight values was 300 μs. The experimental variances of these results were 80 and 90 μs. The fact that the distribution of the resulting values was close to the normal one made it possible to conclude about a purely statistical nature of the variance. This assumption leads to the total accuracy estimation as $\delta t = \frac{\Delta t}{\sqrt{N}}$, where $\Delta t = 85 \mu s$ is the accuracy of one measurement and N = 60, which gives the estimate of $\Delta t \approx 11 \mu s$.

1.11. Experiment on the observation of neutron diffraction by surface ultrasonic waves

In collaboration with IPMT RAS (Chernogolovka) and Max Planck Institute (Munich, Germany) an experiment to observe neutron diffraction by surface ultrasonic waves was performed. The measurements were made on the N-REX reflectometer at the FRM II reactor, neutron wavelength of 4.3 Å.

A single crystal of lithium niobate (LiNiO3) was used as a sample. On its surface two interdigital transducers with a base frequency f = 69 MHz were designed using photolithography. They generated surface acoustic waves (SAW) in each of two directions. Under the application of voltage to the two transducers, a standing ultrasonic wave was produced on the surface.

The area of wave propagation was a stripe with a width of 6 mm and length of 60 mm. The SAW speed was 3590 m/s, about four times higher than the neutron velocity along the sample surface. The experiment was performed with SAW travelling in and against the direction of neutron wave propagation, as well as for the scattering by a standing ultrasonic wave. In all cases, an energy transfer to the neutron took place. If in the case of a travelling wave the phenomenon can be interpreted in terms of a quasi-classical Doppler frequency shift, then in the case of standing waves one deals with a non-stationary quantum effect. Thus, the given study expands a relatively short list of non-stationary quantum experiments with neutrons.

Figures 1-III-18 (a) and (b) shows a result of the measurement in the case of the opposite propagation direction for SAW and neutrons. In the right figure, the stripes of the diffraction scattering from SAW are clearly visible. **Figure 1-III-18 (c)** presents a similar picture for the case of neutron scattering by a standing wave. The stripes of the first order corresponding to the energy transfer $\Delta E = \pm \hbar \Omega$ are seen together with a stripe of the second order with the change in the neutron energy $\Delta E = -2\hbar\Omega$, where $\Omega = 2\pi f$. The value of the quantum of energy in the conditions of this experiment was $\Delta E_0 = \hbar\Omega = 3.276 \times 10^{-7} eV$ We emphasize that here one deals with a non-stationary energy transfer, and purely diffraction beam splitting on a surface structure periodic in space is much smaller than the observed effect.

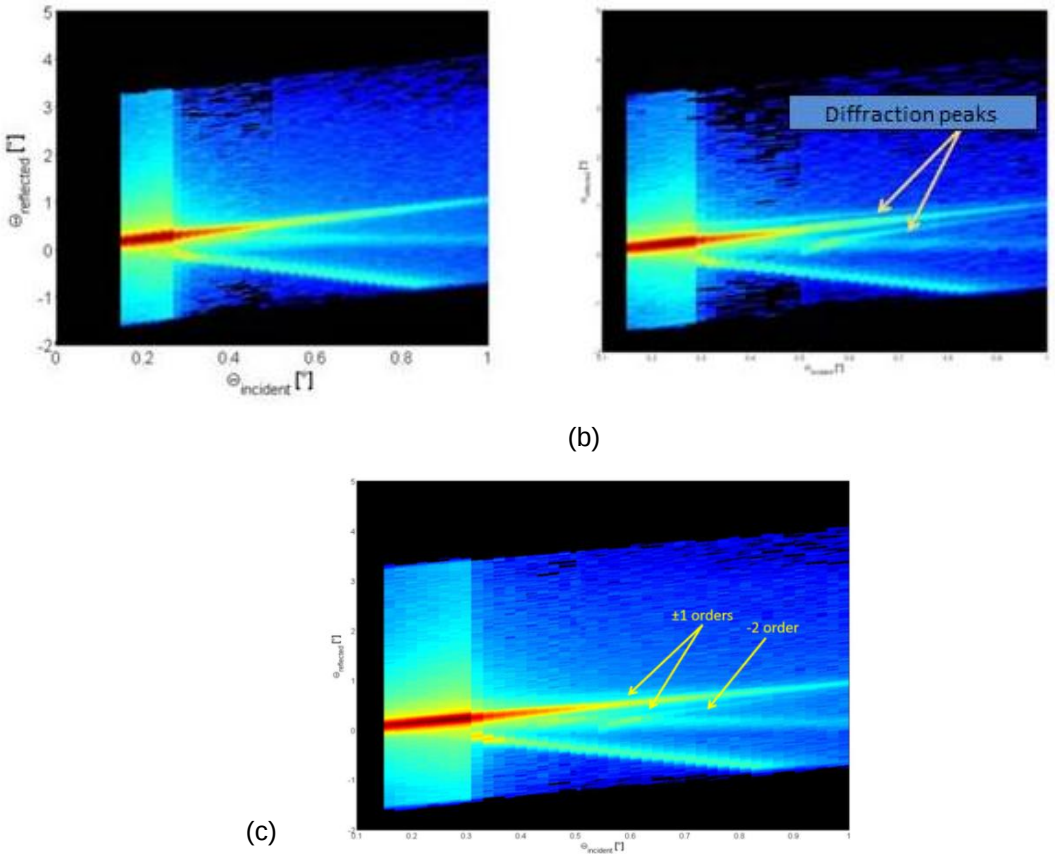

(a) (b)

(c)

Fig. 1-III-18. *2D map of neutron scattering from the surface of lithium niobate in the absence* ***(a)*** *and after generaton* ***(b)*** *of surface ultrasonic waves.* ***(c)*** *2D map of neutron scattering from the surface of lithium niobate in the case of standing SAW.*

1.12. Preparation of the experiment to observe the interaction of UCN with an oscillating barrier at giant accelerations

The purpose of the upcoming experiment is to verify the validity of the model of the effective potential at giant accelerations of the sample. An important step in the preparation of the experiment is quantum calculations of the interaction of the neutron wave packet with a potential structure oscillating in space at different magnitudes of the maximum acceleration of the object $w_{max} = A(2\pi f)^2$, where A and f are the oscillation amplitude and frequency, respectively. The calculations for the case of an oscillating potential barrier have shown that for the case of interest $w_{max} \approx 10^8 cm/s^2$ the observed non-stationary effects for the past state are very small. The calculations for the case of an oscillating resonant structure representing two barriers and a hole between them have revealed that in a wide range of amplitudes and frequencies in the past state, there are visible oscillations in the count rate. As a result, this geometry is selected as a priority geometry for further research. Possible approaches to the designing of the experiment to test the validity of the model of the effective potential at giant accelerations of the sample, have been considered.

The realization of the experiment requires samples whose surface can oscillate without significant deformations in a frequency range from 100 kHz to several MHz. We solve this problem in two ways. First, in collaboration with the Institute of Laue-Langevin the study of the topography

of the sample surface oscillating in space is in progress. Second, the experimental study of oscillating samples is under preparation. For this purpose, a special stand (vibrometer) for mapping the surface of oscillating samples (**Fig. 1-III-19**) has been designed. It consists of a laser interferometer and a two-coordinate table.

Fig. 1-III-19. *Two-coordinate laser vibrometer.*

The setup will make it possible to measure the surface shape synchronously with the phase of the sample movement. At present, the work to create and debug the mathematical software of the stand is underway.

2. Theoretical investigations

The characteristics of a spin-wave neutron interferometer (which consists of a pair of magnetic mirrors placed in a magnetic field non-collinear to the magnetization of the mirrors) in a magnetic field, have been investigated. The setup can be used for studying the properties of the neutron wave packet, as well as for measuring the scattering density correlations in thin films. On the basis of experimental data, the spectrometer sensitivity and the coherent neutron length have been estimated. The possibilities of using spin-echo spectroscopy to determine the coherent neutron length have been considered.

Contrary to the common opinion that the bound states always have discrete spectra, it has been shown that in the hydrogen atom there may be bound singular states with a continuous spectrum. The role of these states in the possible nuclear reactions of cold fusion and processes of star ignition has been discussed.

In the EPR paradox, a question on particle polarizations is under discussion: whether the source emits pairs of flying particles in an entangled state or in the form of individual particles with their own polarizations. To answer this question, a simple Bell's inequality for photons has been proposed. It can be tested in one measurement. A result of the possible measurement is being calculated taking into account the experimental constraints.

The concept of the coherence length of the neutron has been under consideration including the generally accepted definition of a Gaussian wave packet based on the beam formation method and a singular de Broglie wave packet of an individual neutron. Experiments to measure the coherence length have been proposed.

An explanation of the experimentally found small heating of UCN during the storage in traps has been proposed on the basis of the neutron wave packet properties. Due to the finite width of the packet, the transmission and reflection probabilities are accompanied by an increase and

decrease in the energy, respectively. The energy changes at the subcritical incidence of the de Broglie wave packet has been analytically calculated.

3. Methodological and applied research

3.1. Determination of the elemental composition of friable ores

The aim of the work is to study the technical possibilities of measuring the composition of friable ores using in real-time the technology of neutron activation analysis (NAA). In the framework of this study, the following tasks have been formulated: investigation of the influence of the type of gamma-ray detectors on the accuracy of the elemental composition determination for ore samples using Am-Be/Pu-Be sources; analysis of the impact of the position of neutron sources and detectors relative to the sample on the elemental composition determination accuracy; determination of optimal geometries for the equipment location relative to the sample; design of the logical circuit for processing signals from detectors; preparation of the primary design documentation.

In **Table 1-III-1** the rock composition determined by chemical analysis is given.

Table 1-III-1. *Composition of the rock used in the study.*

Results of analyses of ore elemental composition		
Controlled compound	Apatite concentrate, weight %	Tailings, weight %
P_2O_5	38,98	0,9
Al_2O_3	0,99	20,88
CaO	50,58	4,9
SiO_2	2,38	42,16
Fe_2O_3	0,68	8,02
K_2O	0,24	6,02
H_2O	0,06	0,15
TiO_2	0,33	2,92
Na_2O	0,5	10,26

For the study, a PuBe neutron source with the intensity of ~$5*10^6$ n/s was used. **Figures 1-III-20 (a) and (b)** shows a schematics of the experimental setup.

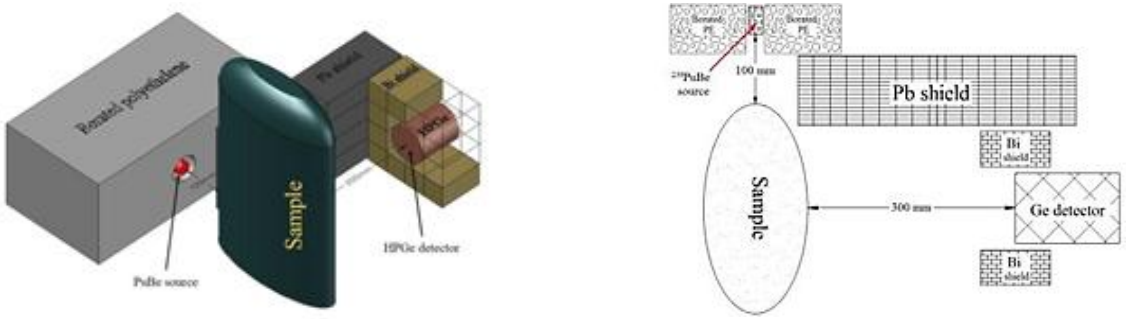

(a) (b)

Fig. 1-III-20. (a) *3D representation of the experimental setup;* ***(b)*** *Experimental setup for determining the elemental composition of friable ores using an HPGe detector.*

1. SCIENTIFIC RESEARCH

At the first stage, gamma-ray spectra of three irradiated ore samples with the content of P_2O_5 – 38, 98, 0,9% and their mixtures were measured using an HPGe detector. **Figure 1-III-21** shows the corresponding spectra for these samples.

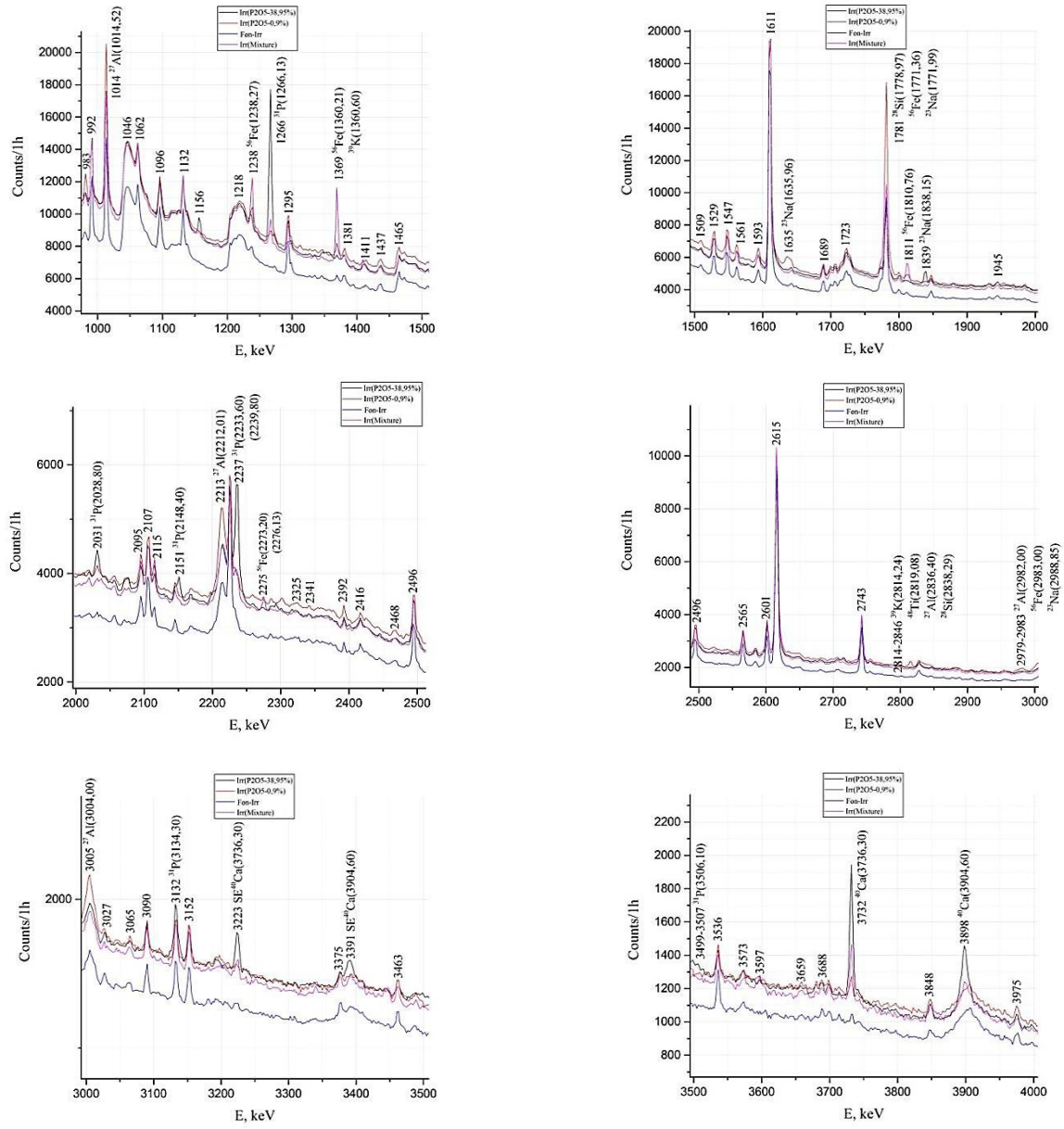

Fig. 1-III.21. *Amplitude distributions of the events recorded by an HPGe-detector for ore samples (apatite concentrate, tailings and their mixtures) irradiated by neutrons from a PuBe-source. Background distributions of the recorded events obtained with the PuBe-source in the absence of the irradiated sample.*

As one can see in the given spectra, there is a clearly observed difference in the results of the measurements of phosphorus (lines 1266 keV and 2237 keV) and calcium (lines 3732 keV and 3898 keV) contents, corresponding concentrations are at the levels of 38 and 0.9% (phosphorus) and 50 and 4.9% (calcium). This demonstrates the possibility of using the presented technique for

determining phosphorus and calcium concentrations with an accuracy that meets the requirements in the industrial extraction of ores of this class.

At the second stage, the measurements of gamma-spectra were made for the specified irradiated samples using a scintillation detector based on a BGO crystal.

A schematic of the experiments using a BGO-detector is given in **Fig. 1-III-22**.

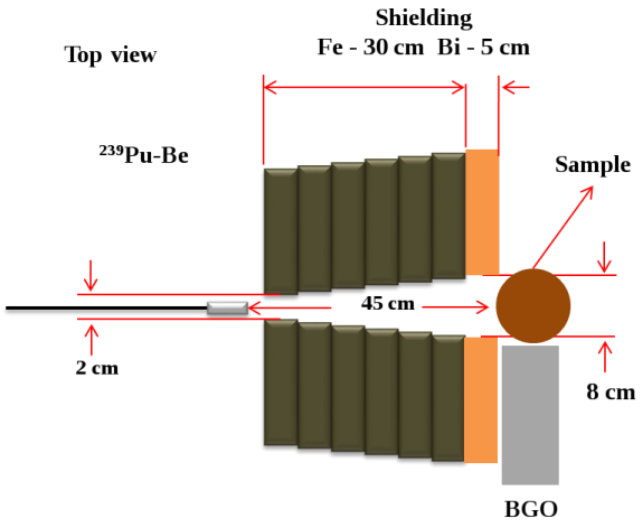

Fig. 1-III-22. *Experimental setup for determining the elemental composition of friable ores using a BGO-detector.*

In **Fig. 1-III-23**, the spectra of events recorded by HPGe and BGO detectors are given for comparison.

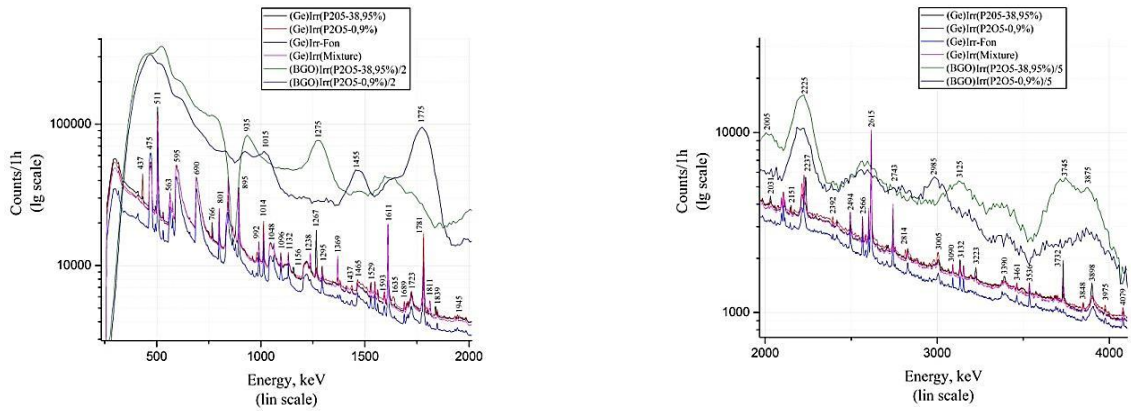

Fig. 1-III-23. *Comparison of the amplitude distribution of events recorded by BGO- and HPGe-detectors.*

As one can see in **Fig. 1-III-23**, there is no sufficiently clear difference in the results of the measurements of the content of phosphorus (lines 1266 keV and 2237 keV) and calcium (lines 3732 keV and 3898 keV) obtained using the BGO-detector as compared to the HPGe-detector. This is due to an essentially worse energy resolution and higher background for the BGO-detector in comparison with the HPGe-detector.

Nevertheless, BGO-detectors can still be used in measurements of the elemental content of friable ores. For this purpose, at this stage it is necessary to develop and create a highly efficient algorithm for the analysis of experimental data.

It is worth considering the question of using a gamma-ray detector based on $LaBr_3$($LaCr_3$) crystals.

3.2. Determination of the relative humidity of coke

The aim of this experiment is to verify the technical possibility of using detectors based on BGO and NaI (Tl) crystals and standard neutron sources for real-time determinination of the humidity of coke and other friable materials for industrial purposes. The method is based on the interaction of neutrons with hydrogen and oxygen nuclei constituting water molecules. Hydrogen effectively reacts with slow neutrons through the neutron capture, thereby forming deuterium, which emits 2223-keV gamma-rays. The main reaction for fast neutrons interacting with oxygen is inelastic scattering. In the process a cascade of characteristic gamma-rays is emitted with the most notable line at 6129 keV. These two lines were used for analysis of water content in the sample.

The studied sample is a closed volume of coke (coal). **Figure 1-III-24** shows a schematic of the experiment. A ^{239}PuBe neutron source with the intensity of ~ 5*10^6 n/s is used for irradiating the sample. Gamma-rays from the sample were measured by the NaI or BGO detectors. A combined shield was installed between the detector and the neutron source to prevent the exposure of the detector to direct neutrons. To test the method, we used a sample weighing about 3 kg, to which water was added to the content from 2% to 80%.

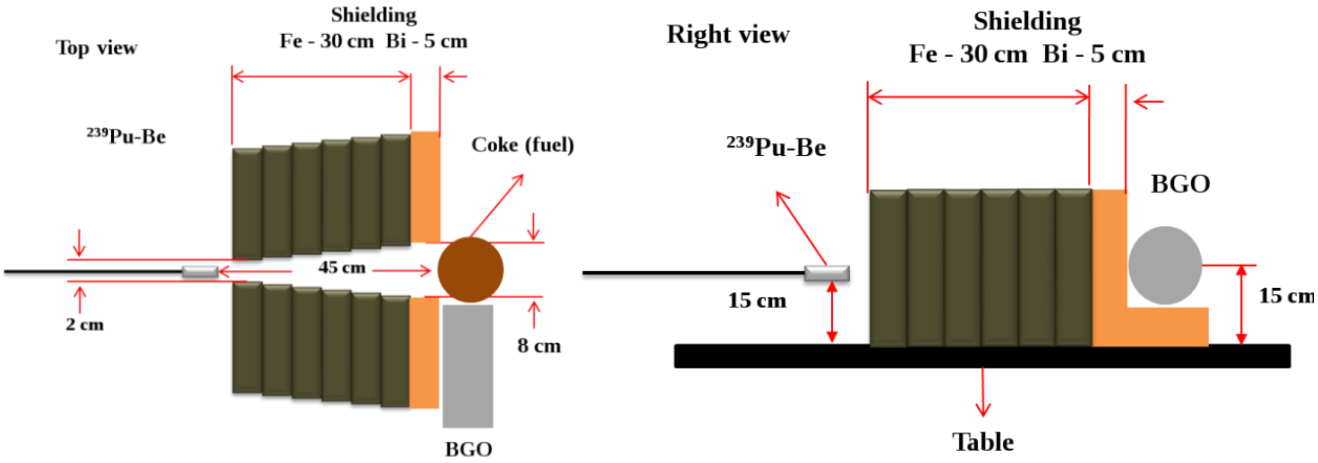

Fig. 1-III-24. *The experimental setup for determining water content in samples (top view and right side view).*

Figures 1-III-25 and **1-III-26** show the spectra of gamma-rays with the energies of 2223 keV and 6129 keV and their analysis for the water content of 6% and 42%, respectively.

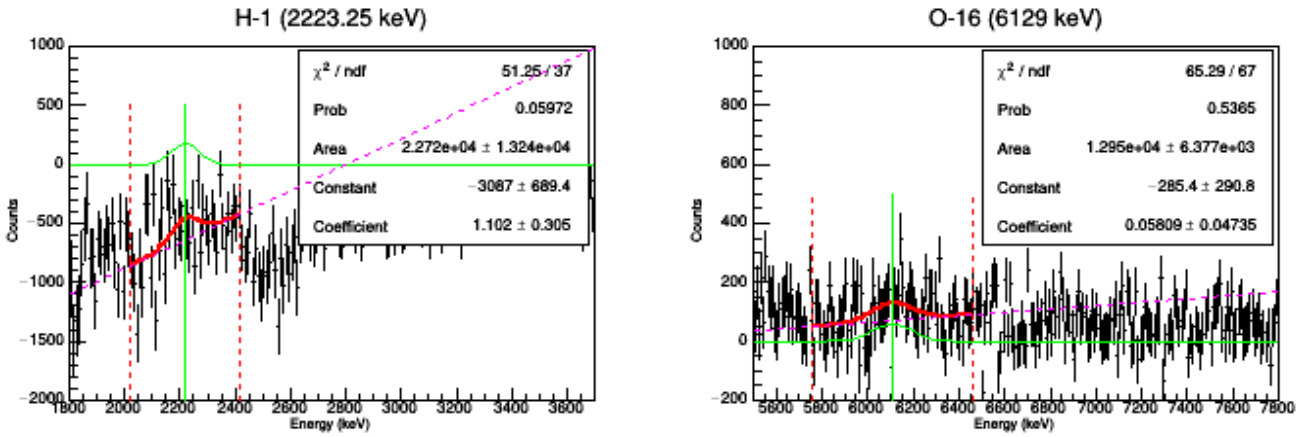

Fig. 1-III-25. *Water content of 6%.*

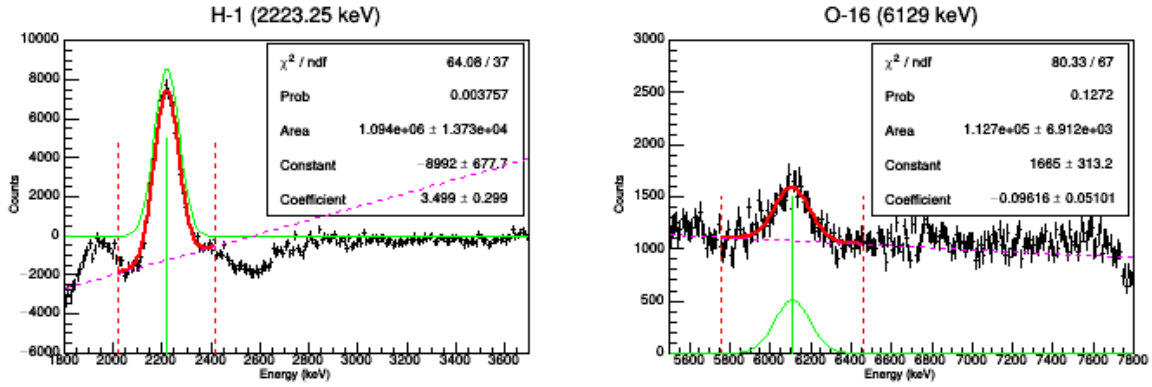

Fig. 1-III-26. *Water content of 42%.*

Figure 1-III-26 illustrates the dependence of the intensity of gamma-lines on the water content in the sample.

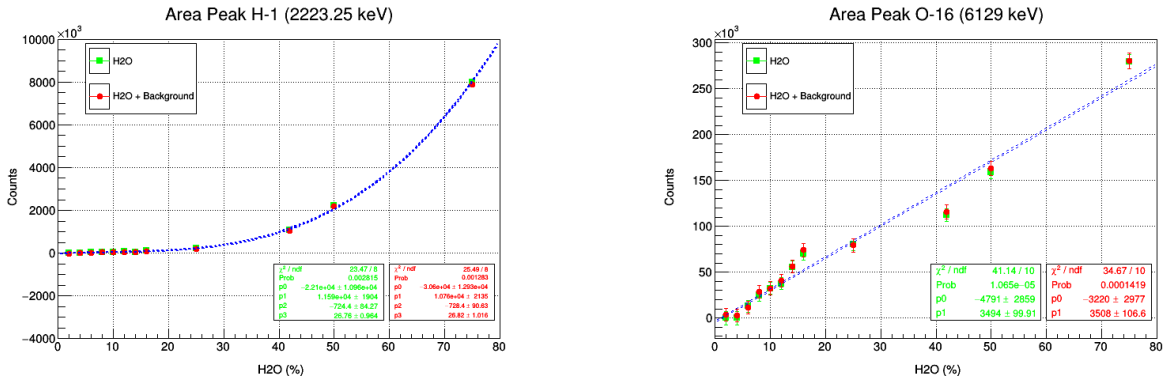

Fig. 1-III-26. *Intensity of gamma-lines of 2223 keV and 6129 keV as a function of water content in the sample.*

Thus, it has been demonstrated that the water content in coke can be determined by this method starting from the humidity of 5%. For industrial purposes, a higher accuracy is required. Therefore, these studies are planned to be continued to achieve the accuracy within 0-5%.

3.3. Analytical investigations on charged particle beams of the EG-5 accelerator

The research of elemental depth profiles of near-surface layers in various samples was the main direction of activity in 2016. The analytical studies were performed on the beams of charged particles with the energy from 1.0 MeV to 3.1 MeV using a variety of nuclear-physical analytical techniques including Rutherford backscattering (RBS), elastic recoil detection (ERD) and particle induced X-ray emission (PIXE). The investigations were carried out in collaboration with Moscow State University (Moscow), LETI (Saint-Petersburg), VSU (Voronezh), UMCS (Lublin, Poland), Institute of Electrical Engineering, Slovak Academy of Sciences (Bratislava), Institute of Physics, Vietnam Academy of Science and Technology (Hanoi, Vietnam). The changes in the elemental composition of the near-surface layers of GaAs crystal samples doped with different doses of heavy Ar^+ and Xe^+ ions were studied. In addition, the composition, structure and morphology of the surface of nanosized platinum-containing silicon films synthesized by the sol-gel technology were investigated. The influence of the irradiation by Xe^+ ions and neutrons on the structural characteristics of SiC and SiC(N) films prepared by the PECVD (Plasma Enhanced Chemical Vapour Deposition) technique was studied.

3.4. Analytical investigations at the IBR-2 reactor

In 2016, the REGATA facility was used for multi-element instrumental neutron activation analysis of about 3,000 environmental samples (vegetation, soil, air filters), a number of technological, biological and archaeological samples, as well as of samples of extraterrestrial origin in the framework of programs and grants of the JINR Member States and Protocols on scientific and technical cooperation with the JINR Non-Member States. Investigations of test samples were conducted for an interlaboratory comparison of the results under the IAEA program.

3.4.1. Development of the NAA&AR experimental base

Development of the software package for complex automation of multi-element neutron activation analysis (NAA) at the IBR-2 reactor was continued in 2016 (Pavlov et al., 2016). Work on the automation of NAA was carried out in the framework of the IAEA Coordinated Research Project «Development of an Integrated Approach to Routine Automation of Neutron Activation Analysis" (F1.20.25/CRP1888, Contract No. 17363).

3.4.2. Biomonitoring of air pollution

In 2016, the summing-up of the activities conducted in 2010-2015 in the framework of the international program "Heavy metal atmospheric deposition in Europe – estimations based on moss analysis" was done (Schroeder et al., 2016). In cooperation with the Laboratory of Information Technologies of JINR a cloud system has been developed to collect, store and process information on biomonitoring of atmospheric deposition of heavy metals and other toxic elements in the framework of the UN Programme on air of Europe (Ososkov, Frontasyeva et al., 2016). The comparison of moss species that grow in arid regions has become an important stage in this research. We have determined the species that have the same accumulating capacity as the three species used in the ICP Vegetation program (Gorelova, Frontasyeva et al., 2016). In the framework of the Serbia-JINR Cooperation Program a comparative analysis of air pollution in the so-called "street canyons" in Moscow and Belgrade has been performed (Goryainova et al., 2016). In cooperation with the Polish and French institutions a study of peat columns from Siberia was published in NATURE (Scientific Reports) (Fiałkiewicz-Kozieł et al., 2016).

3.4.3. Biotechnologies

In 2016, in collaboration with the Institute of Microbiology and Biotechnology of the Academy of Sciences of Moldova a new method of synthesis of selenium nanoparticles by cyanobacteria *Spirulina platensis* and *Nostoc linckia* was developed. Along with a number of optical and analytical methods, we used the neutron activation analysis at the IBR-2 reactor to characterize the selenium accumulation process by these cyanobacteria. The assessment of changes in the biochemical composition of cyanobacterium biomass (proteins, carbohydrates and others) in the process of selenium nanoparticles formation has been performed as well (Zinicovscaia, Chiriac et al. 2016, Zinicovscaia, Rudi et al. 2016). In 2016, work continued on the study of processes of extraction of toxic metals from wastewater using microalgae *Spirulina platensis* (Zinicovscaia, Cepoi et al. 2016). In collaboration with Institute of Experimental Physics, SAS in Košice a study on the extraction of heavy metals from model solutions using poplar sawdust was performed (Demcak et al., 2016). In cooperation with the University of Oulu, Finland, the application of NAA for analysis of pine sawdust used in wastewater treatment as a sorbent of metals has been studied (Keränen et al., 2016). In collaboration with the A.N. Frumkin Institute of Physical Chemistry and Electrochemistry of RAS in the framework of the projects supported by RFBR (15-05-08919 and 15-33-20069) work has been performed to study the processes of accumulation and biosorption of metals (vanadium, chromium, uranium, lanthanum) from mono- and multicomponent systems by microalgae *Spirulina platensis* and bacteria *Pseudomonas putida*. The results obtained showed that the concentrations of metals accumulated by the microbial biomass in the process of bioaccumulation were 15-40 times higher than in the biosorption process (Zinicovscaia, Safoniov et al. 2016). Studies have been conducted for biosorption of 13 metals by three types of organisms: bacteria, microalgae and yeast aimed at determination of the most effective sorbent for each metal. In cooperation with the Scientific-Production Association "Biosolar MSU", work has begun on the application of NAA to assess the efficiency of iodine and zinc accumulation by microalgae *Spirulina platensis* for industrial production of iodine- and zinc-containing medicines.

3.4.4. Environmental assessment

In 2016, work on the evaluation of industrial pollution of agricultural soils in one of the satellite cities of Cairo (Sadat City) was completed (Badawy et al., 2016). To continue the work on the assessment of the environmental situation in the basin of the Nile River and its delta, an additional neutron activation analysis of soil and sediment samples from the area of the Central Nile has been performed, and a statistical analysis of the whole amount of the results obtained earlier and in 2016 has been carried out. In collaboration with the National Research Center in Dokki, Cairo, work on modeling the coordinate bonds of several elements (Na, Mg, Ca, Fe, Ni, and Zn) with organic acids has been completed (Okahsa et al., in press). In 2016, the NAA of coral samples from the Red Sea as well as of brown and red algae from the Egyptian coastal aquatic areas of the Mediterranean sea was carried out in the framework of the Protocol on Cooperation with Cairo University. In collaboration with the A.O. Kovalevsky Institute of Marine Biological Research (Sevastopol) the analysis of the samples of macroalgae-biomonitors (red, green and brown) collected in the coastal zone of the Black Sea for the assessment of the state of the Crimea coastal ecosystem has been completed. The study of the seasonal variation of concentrations of 46 elements in the phytoplankton of coastal areas of the Black Sea has been completed. The obtained results have shown that phytoplankton can be successfully used as a biomonitor of aquatic ecosystems. In 2016, in cooperation with Moscow State University (Faculty of Biology) the investigation on the determination of the elemental composition of soil, bottom sediments, terrestrial and aquatic vegetation to assess the transport of pollutants in the strategically important areas of the Black Sea (coastal area of Anapa, Novorossiysk and Tuapse) was completed (P.Nekhoroshkov et al, 2016).

3.4.5. Material Sciences

In 2016, in the framework of the BRFBR-JINR joint grant and in cooperation with the Scientific and Practical Materials Research Center of the National Academy of Sciences of Belarus, the investigations of the crystallization processes and the characterization of artificial diamonds in the C-Mn-Ni-Fe system were conducted (Aleksiayenak et al., 2016). The NAA of 56 samples related to the topic "Studies on the phase formation and physical characteristics of the compounds in the Cu-Fe-S system at high pressures and temperatures" was carried out. Work has begun with the Institute of Nuclear Sciences "Vinca" in Belgrade (Serbia) to study the elemental composition of spider silk, which is of great interest both from the scientific and practical points of view.

3.4.6. Analysis of food products

The determination of mercury intake from the consumption of fish and seafood has been completed. This study carried out in collaboration with the specialists from the Analytical Center of the Geological Institute, Russian Academy of Sciences (Gorbunov et al., 2016).

3.4.7. Geology

In the framework of the joint JINR-Romania project, unconsolidated sediments of the western slope of the Romanian shore of the Black Sea have been studied in 2016 (Duliu, G.Oaie et al., 2016).

3.4.8. Archeology

Nine icons of the second half of the XVIII and XIX centuries, from different regions of Romania and Russia have been studied in detail using the epithermal neutron activation analysis (ENAA), X-ray fluorescence analysis (XRF), digital radiography (DR), Fourier transform infrared spectroscopy (FTIR) and IR-Raman spectroscopy. These methods were used to determine the chemical composition of pigments, as well as deeper layers of icons, while FTIR spectroscopy allowed us to identify the nature of binders. The results of this work have demonstrated the importance of the use of different methods for studying such complex objects as icons (Duliu, Sister Serafima (Dorina-Claudia Samoilescu) et al., 2016).

3.4.9. Analysis of materials of extraterrestrial origin

In 2016, a multi-element NAA of ferrous and carbonaceous meteorites received from the United States and Serbia was performed. For the first time, iridium content was determined in exotic clay samples from Serbia (originally from famous Fish Clay in the sea shore at Stevns Klint in Denmark). Most researchers believe that their Ir enrichments (on a ppb level) resulted from the impact of a chondritic asteroid striking the Earth at that time (about 65 millions years ago). Our results evidence for that hypothesis.

3.4.10. Medical plants

In 2016, we continued investigations in a new promising line of research – determination of the elemental composition of plants used in medicine. These studies are conducted in cooperation with the specialists from Mongolia, Bulgaria (Vasilev et al., 2016), Poland, China (Li Xuesong et al., 2016) and Portugal.